Research Square

Preprints are preliminary reports that have not undergone peer review.
They should not be considered conclusive, used to inform clinical practice,
or referenced by the media as validated information.

Preparation and Resource Utilization of Lightweight Ceramsite from High-Chlorine Medical–Municipal Co-Incineration Ash and Tuff

Junyang Teng

jteng89@hotmail.com

NanYang Medical College https://orcid.org/0009-0002-3680-7255

Yonghao Yang

Chongqing Jiaotong University

Fei Xu

NanYang Medical College

Research Article

Keywords: medical-municipal co-incineration, fly ash, tuff, lightweight ceramsite, heavy metals, resource utilization

Posted Date: October 30th, 2026

DOI: https://doi.org/10.21203/rs.3.rs-10896805/v1

License: This work is licensed under a Creative Commons Attribution 4.0 International License.
Read Full License

Preparation and Resource Utilization of Lightweight Ceramsite from High-Chlorine Medical–Municipal Co-Incineration Ash and Tuff

Junyang Teng [a*], Yonghao Yang [b], Fei Xu [a]

a Nanyang Medical College, Nanyang 473000, China

b Chongqing Jiaotong University, Chongqing 400074, China

* Corresponding author.

E-mail addresses: jteng89@hotmail.com (J. Teng), 814465545@qq.com (Y. Yang), 577895291@qq.com (F. Xu)

Abstract

Purpose: Medical–municipal co-incineration fly ash is hazardous because of its high chlorine and Pb/Cd contents. This study converted it into lightweight ceramsite together with bottom ash and tuff and tracked the chlorine and heavy-metal behavior during washing and sintering.

Methods: The fly ash was dechlorinated by three-stage countercurrent water washing and then sintered with bottom ash and tuff. Single-factor experiments and Box–Behnken response-surface design optimized the formulation and firing schedule. XRD, SEM–EDS, Tessier extraction, and leaching tests characterized the product.

Results: The optimal formulation was 20% fly ash with a bottom ash-to-tuff ratio of 40:60, preheated at 500 °C for 20 min and sintered at 1100 °C for 10 min. The 900-grade ceramsite showed a particle strength of 2014 N and a bulk density of 890 kg/m³. Washing removed 96.2% of the chlorine, and 82.2% of the chlorine entering the sintering stage was released to the flue gas. Preliminary balances indicated that 70–85% of Pb, Cd, and Zn remained in the ceramsite.

Conclusion: The proposed route provides a technically feasible basis for resource recovery of high-chlorine co-incineration fly ash, provided that flue-gas deacidification is implemented and heavy-metal retention is verified by standard sampling.

Keywords

medical-municipal co-incineration; fly ash; tuff; lightweight ceramsite; heavy metals; resource utilization

1 Introduction

Medical waste contains pathogens, toxic chemicals, and heavy metals and demands careful handling throughout its life cycle. Incineration remains the preferred treatment in many regions because it inactivates pathogens and greatly reduces waste volume. In China, medical waste generation has grown with the expansion of healthcare services [1, 3]. Centralized plants increasingly co-incinerate medical waste with municipal solid waste to improve efficiency and reduce operating costs [1, 3]. This mode is encouraged by national policies and is expected to remain dominant in large and medium-sized cities [2, 3]. The resulting fly ash is hazardous. It concentrates Pb, Cd, Cr, chloride salts, and chlorinated and brominated organics [1–4]. Co-incineration mixes these pollutants with those of municipal waste. The residue is therefore more variable and harder to manage than ash from a single feedstock. Landfilling is also constrained by land scarcity and stricter environmental requirements [2, 30].

Several treatment routes have been explored for this residue. Chemical stabilization and cement-based solidification are effective but costly, and the products may release metals under acidic conditions or after

long service. Geopolymer binders consume less energy and carbon [7, 8], yet they do not remove chloride or dioxin-like compounds [1]. Thermal treatment offers a different balance. It can fix metals in newly formed mineral phases, destroy organic contaminants, and convert the residue into a reusable construction material. The main drawback is energy input, which can be offset by adding silica- and alumina-rich raw materials [5, 6, 9–11]. Sintering fly ash into ceramsite is therefore attractive because the product is a marketable lightweight aggregate with established uses in lightweight concrete, insulation, and horticulture [21].

Chlorine is the decisive pollutant in this system. Co-incineration fly ash commonly contains 10–20 wt.% chloride, mainly as soluble NaCl, KCl, and $CaCl_2$, most of which can be removed by water washing [15, 25, 26]. If chloride is retained during firing, it promotes the volatilization of Pb, Cd, and Zn through chlorination reactions. These metals are then shifted to the flue gas, creating secondary pollution [4, 15]. HCl released during sintering likewise requires flue-gas treatment. Residual chlorine can persist as soluble salts or form chlorosilicate and chloroaluminate phases in the product [15]. High-chlorine co-incineration ash therefore cannot simply be processed with the formulations and firing schedules developed for ordinary municipal solid waste incineration fly ash. The fate of chlorine, from raw ash through product to flue gas, must be quantified [4, 15, 26].

Ceramsite production from incineration fly ash has attracted growing attention. Shao et al. [9] showed how heavy metals are immobilized in fly ash-based ceramsite. Wu et al. [10] co-sintered fly ash with ferronickel slag, and Long et al. [11] used a $CaO–SiO_2–Al_2O_3$ system with clay to produce high-strength aggregates. Han et al. [18–20] demonstrated that water washing and bloating agents improve aggregate quality and metal retention. Other studies have evaluated the environmental risk of such products [12, 22] and their use in concrete [21]. Together, these works confirm the technical feasibility of fly ash ceramsite. Three gaps remain, however. First, nearly all earlier studies used municipal solid waste incineration fly ash alone. High-chlorine, high-Pb/Cd co-incineration ash has seldom been examined during washing and sintering [9–11, 16, 17]. Second, most studies relied on leaching tests alone and did not follow chlorine or volatile metals through firing. Such data are needed to distinguish true immobilization from transfer to the flue gas [4, 15, 19]. Third, the compatibility of co-incineration ash with tuff has not been established. Tuff is a silica- and alumina-rich volcanic rock that has performed well as a framework component for lightweight aggregates and geopolymers [23, 24]. The formulation, firing window, phase evolution, and environmental performance of this ash–tuff system therefore remain open questions.

Tuff is an abundant volcanic rock rich in reactive silica and alumina and has already been used to prepare alkali-activated materials and lightweight aggregates [23, 24]. In a previous project, bottom ash and tuff blended with 20% municipal waste incineration fly ash were sintered into a 900-grade lightweight ceramsite with adequate strength and acceptable leaching. That work used ordinary municipal ash. It did not address the high chloride and Pb/Cd contents of medical–municipal co-incineration fly ash, for which water washing is usually required [25, 26]. The present study extends this route to co-incineration ash and sets four objectives. The first is to establish a water-washing and ternary-blending procedure for lightweight ceramsite preparation. The second is to optimize the formulation and firing schedule through single-factor experiments and Box–Behnken response-surface design. The third is to characterize the phase composition, microstructure, and heavy-metal leaching behavior of the product. The fourth is to construct preliminary chlorine and heavy-metal mass balances across the washing–sintering route.

2 Materials and methods

2.1 Materials

Co-incineration fly ash was collected from the bag filter of a medical–municipal co-incineration plant (daily capacity ≥800 t/d; medical-waste ratio 5–10%). The sample was dried at 105 °C for 24 h and ground

to pass a 100-mesh sieve. Its chemical composition and heavy-metal contents are given in Table 1 and Table 2, respectively. The fly ash was rich in CaO (34.2%) and Cl (19.8%) but contained only 18.6% SiO_2 + Al_2O_3 in total, indicating that it could not be used alone as an aluminosilicate precursor.

After drying and grinding, the fly ash was homogenized by quartering to obtain representative subsamples for chemical analysis. XRF analysis was performed on fused beads prepared from ignited powder, and the loss on ignition was determined at 950 °C. Total heavy metals were digested with HNO_3 and HF in a microwave system following USEPA Method 3052 and measured by ICP-OES or ICP-MS.

Table 1 Chemical composition of the co-incineration fly ash (wt.%)

Component	CaO	SiO_2	Cl	SO_3	Al_2O_3	Fe_2O_3	Na_2O	K_2O	MgO	P_2O_5	TiO_2	Others
Content	34.2	16.8	19.8	13.5	1.8	3.9	3.5	2.6	1.8	1.2	0.6	Balance

Table 2 Total heavy-metal contents of the co-incineration fly ash (mg/kg)

Element	Pb	Zn	Cd	Cr	Cu	Mn	Ni	As
Content	5120	7800	245	720	1340	800	280	85

Bottom ash was collected from the grate outlet of the same plant, crushed, ground to pass a 100-mesh sieve, and dried at 105 °C. Tuff was obtained from a volcanic tuff mine, crushed, ball-milled, sieved, and dried under the same conditions. Table 3 lists their chemical compositions. The tuff contained 79.94% SiO_2 + Al_2O_3 and therefore served as the main framework-forming precursor. Its K_2O content of 8.88% was consistent with the presence of K-feldspar, indicating a potassium-rich volcanic rock. The loss on ignition of the bottom ash was approximately 5.2%, and loss on ignition was reported separately from the oxide totals.

The bottom ash and tuff were homogenized by quartering after crushing and sieving. The oxide totals in Table 3 were normalized to 100 wt%, and the loss on ignition was reported separately to avoid double counting with the oxide components.

Table 3 Chemical compositions of bottom ash and tuff (wt.%)

Component	SiO_2	Al_2O_3	CaO	Fe_2O_3	Na_2O	K_2O	MgO	SO_3	TiO_2	Cl	Others
Bottom ash	42.6	15.3	21.8	6.8	4.2	3.5	2.6	1.8	—	0.51	0.89
Tuff	67.36	12.58	6.75	1.86	1.45	8.88	0.53	—	0.26	0.20	0.13

2.2 Water-washing dechlorination

Because the fly ash contained 19.8% Cl, a three-stage countercurrent water-washing process was applied before sintering. The liquid-to-solid ratio was 8:1 mL/g, the water temperature was 60 °C, and each stage lasted 20 min, with solid–liquid separation between stages. The washed fly ash was dried at 105 °C to constant weight and ground to pass a 100-mesh sieve. Washing reduced the Cl content to about 1.1% and lowered the chlorine load before firing [25, 26]. Based on 200 kg of raw fly ash, the washed fly ash accounted for 135 kg and the dissolved solids for 65 kg. The chlorine mass balance was closed, with 38.115 kg Cl removed in the wastewater and 1.485 kg remaining in the washed ash.

Each washing stage used deionized water at a liquid-to-solid ratio of 8:1 mL/g and a temperature of 60 °C, with continuous stirring for 20 min. The slurry was separated by vacuum filtration after each stage, and the filtrate was collected as washing wastewater. In the countercurrent configuration, fresh water entered the third stage. The filtrate from the third stage was reused for the second stage, and the filtrate from the second stage was reused for the first stage. This configuration maintained a high concentration gradient for chloride dissolution while reducing fresh-water consumption [25, 26]. The combined wastewater was analyzed by ion chromatography to close the chlorine mass balance.

2.3 Ceramsite preparation

Fly ash, bottom ash, and tuff were weighed in the designed proportions and mixed, and the mixture was ground to pass a 200-mesh sieve. Water was added at a liquid-to-solid ratio of 0.3–0.4 mL/g, and the mixture was pelletized into green balls 10–14 mm in diameter. The pellets were dried at 105 °C for 10 h, heated at 10 °C/min to the preheating temperature, and held for 20 min. They were then heated to the sintering temperature, held for the designed time, cooled in the furnace to 100 °C, and finally cooled to room temperature.

Green pellets were formed on a rotating pan granulator by adding water gradually until coherent balls of 10–14 mm were obtained. The moisture content was adjusted so that the mixture could be rolled without sticking. The pellets were dried at 105 °C for 10 h to remove free water and avoid explosive steam release during heating. Heating was performed in air at 10 °C/min in both the preheating and sintering stages. After sintering, the pellets were cooled inside the furnace to 100 °C and then to room temperature to reduce thermal shock and crack formation.

2.4 Experimental design

Single-factor experiments were performed to examine fly ash content, bottom ash-to-tuff mass ratio, preheating temperature, sintering temperature, and holding time (Table 4). On the basis of these results, response-surface optimization was applied to the factors that most strongly influenced particle strength. Particle strength was used as the response, while bulk density, water absorption, and heavy-metal leaching were evaluated separately as constraints. Box–Behnken design was used, and each test was performed in triplicate.

The Box–Behnken design for the three selected factors comprised 17 runs, including five center-point replicates (Table 5), and the run order was randomized with Design-Expert 13.0. The bottom ash-to-tuff mass ratio and preheating temperature were fixed at their optimum levels during the response-surface stage. Particle strength for each run was the average of ten pellets, while bulk density, water absorption, and heavy-metal leaching were measured on triplicate subsamples. Model adequacy was evaluated by analysis of variance, R^2 and adjusted and predicted R^2, adequate precision, and the lack-of-fit test.

Table 4 Factors and levels of the single-factor experiments

Factor	Level 1	Level 2	Level 3	Level 4	Level 5
Fly ash content (%)	10	20	30	40	—
Bottom ash:tuff	25:75	35:65	40:60	45:55	50:50
Preheating temperature	400	500	600	—	—

(°C)					
Sintering temperature (°C)	1050	1100	1150	—	—
Holding time (min)	5	10	15	20	—

Table 5 Factors and coded levels of the Box–Behnken design

Factor	Symbol	Low (−1)	Center (0)	High (+1)
Fly ash content (%)	A	10	20	30
Sintering temperature (°C)	B	1050	1100	1150
Holding time (min)	C	5	10	15

2.5 Characterization and testing

Particle strength, bulk density, apparent density, and 1 h water absorption were determined according to GB/T 17431.2-2010 [27]; particle strength was averaged over ten pellets. Chemical composition was analyzed by X-ray fluorescence spectrometry, phase composition by X-ray diffraction (Cu Kα, 40 kV, 5°–70°), and morphology by scanning electron microscopy with energy-dispersive X-ray spectroscopy (SEM–EDS, 15 kV). Total heavy metals were measured by inductively coupled plasma optical emission spectrometry or mass spectrometry after microwave digestion following USEPA Method 3052.

Leaching tests were conducted according to HJ/T 300-2007 [28] (acetic acid buffer method) and HJ 557-2010 [29] (horizontal shaking method). The former simulated acidic landfill or acid-rain conditions, whereas the latter simulated neutral aqueous contact relevant to construction use. GB 5085.3-2007 [31] was used for hazardous-waste identification, HJ 1134-2020 [30] for fly-ash pollution control, and GB 8978-1996 [32] as a reference limit. Heavy-metal speciation in the raw fly ash was determined by the Tessier five-step extraction, which separated exchangeable, carbonate-bound, Fe–Mn oxide-bound, organic-bound, and residual fractions. Chloride contents in the fly ash, washed fly ash, ceramsite, and flue-gas absorption solution were measured by ion chromatography after water or acid extraction. The detection and quantification limits of ICP-MS were determined from calibration blanks, and all reported leachate concentrations exceeded the quantification limits.

XRD patterns were recorded over 5°–70° (2θ) with Cu Kα radiation, a step size of 0.02°, and a scanning speed of 4°/min. SEM specimens were sputter-coated with gold and observed at 15 kV, with EDS used for semi-quantitative spot analysis. The Tessier procedure used 1 mol/L $MgCl_2$ (pH 7.0), 1 mol/L NaOAc (pH 5.0), and 0.04 mol/L $NH_2OH{\cdot}HCl$ in 25% acetic acid to extract the exchangeable, carbonate-bound, and Fe–Mn oxide-bound fractions. The organic-bound and residual fractions were extracted with H_2O_2 and NH_4OAc and with $HF–HClO_4$ digestion, respectively. Leaching tests were conducted at liquid-to-solid ratios of 20:1 (HJ/T 300-2007) and 10:1 (HJ 557-2010), using the agitation conditions specified in each standard. Chloride in aqueous extracts was measured by ion chromatography against standard solutions.

2.6 Statistical analysis

Each test was performed in triplicate, and the results are reported as mean ± standard deviation. Design-Expert 13.0 was used for response-surface design and analysis of variance, and Origin 2024 was used for plotting and data fitting.

All data processing and plotting were performed in Origin 2024. The response-surface model was verified by confirmatory runs under the recommended conditions, and the predicted and experimental values were compared. A significance level of $p < 0.05$ was adopted for all statistical tests.

3 Results and discussion

3.1 Properties of co-incineration fly ash and water-washing dechlorination

The co-incineration fly ash contained 34.2% CaO, 19.8% Cl, and only 18.6% SiO_2 + Al_2O_3, confirming its high-calcium, high-chlorine, low-silica/alumina character. Total Pb, Zn, and Cd were 5120, 7800, and 245 mg/kg, respectively [1–4]. Tessier speciation showed that 57.8% of Cd occurred as the exchangeable fraction. The weak-bound fractions (F1 + F2) of Pb and Zn exceeded 63% and 55%, respectively, indicating a high potential for release under acid rain or landfill leachate. The XRD pattern and SEM morphology of the fly ash are shown in Fig. 1.

The XRD pattern of the raw fly ash was dominated by calcite, anhydrite, quartz, and the chloride salts KCl and NaCl, consistent with the high CaO, SO_3, and Cl contents in Table 1. SEM observation showed irregular, loosely aggregated particles covered with fine adhered crystals, a morphology typical of bag-filter ash after condensation of volatile chlorides and sulfates [1, 4]. This surface structure is consistent with both the high exchangeable Cd fraction and the rapid dissolution of chloride during water washing [25, 26]. These phases also provide the starting mineralogy for the phase transformations discussed in Section 3.5.

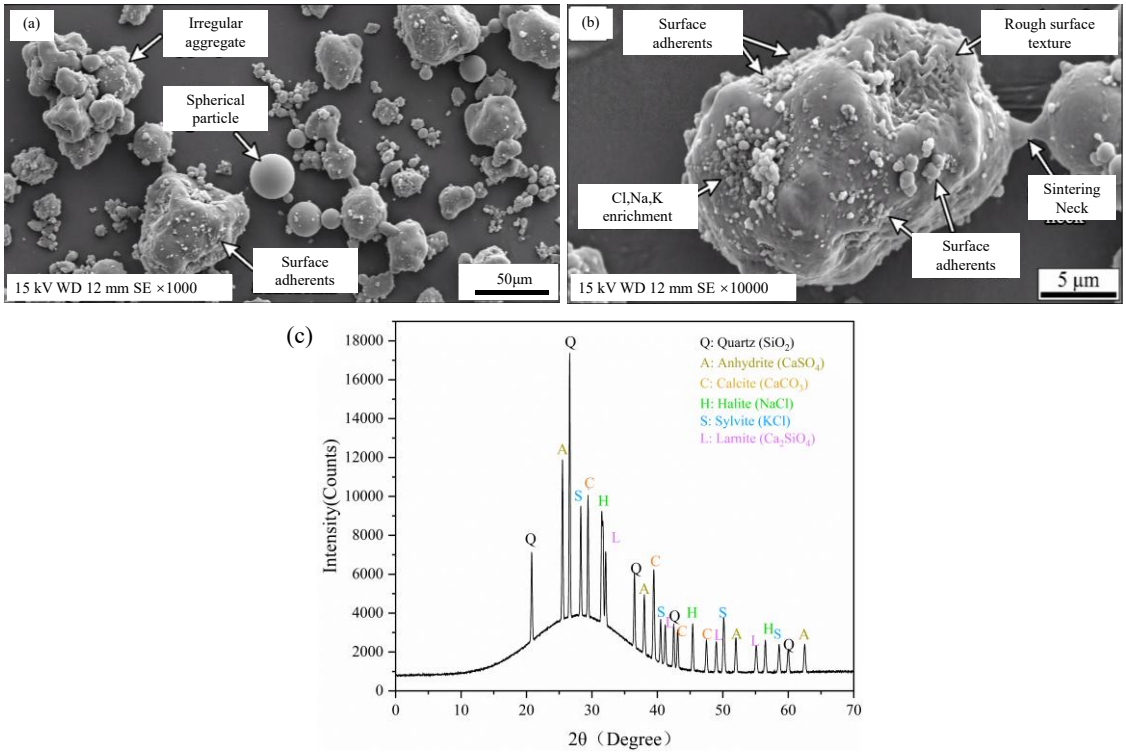

Fig. 1 SEM images and XRD pattern of the medical–municipal co-incineration fly ash: (a) low-magnification SEM image; (b) high-magnification SEM image; (c) XRD pattern

Three-stage countercurrent washing reduced the Cl content from 19.8% to 1.1%. Based on 200 kg of raw fly ash, the washed fly ash mass was 135 kg and the dissolved solids were 65 kg. Chlorine and non-chlorine components were both consistent with this total mass loss. The cumulative dechlorination efficiency was 96.2% on a chlorine mass basis (Fig. 2), and this step reduced the likelihood of metal chlorination volatilization during firing [4, 25, 26]. The removal efficiencies of Pb, Cd, and Zn by washing were only 4.6%, 6.5%, and 2.8%, respectively. These total-mass removal efficiencies should not be directly compared with the change in leachate concentration, which reflects only the mobile fraction.

Water washing removed chloride by dissolving soluble salts rather than by decomposing the ash matrix. The Cl content decreased from 19.8% to 1.1%. The mass loss of 65 kg per 200 kg of raw ash matched the dissolved NaCl, KCl, and $CaCl_2$ together with the fine particles entrained in the filtrate. The total-mass removal efficiencies of Pb (4.6%), Zn (2.8%), and Cd (6.5%) were low, which indicates that these metals are not mainly present as soluble chlorides. This result is not inconsistent with the high Cd leachate concentration. The exchangeable Cd detected by Tessier extraction can be released under acidic conditions, whereas the near-neutral washing water dissolved only a small part of the metal pool [4, 25]. The distinction between total-mass removal and leachability reduction is therefore essential for Section 3.6.

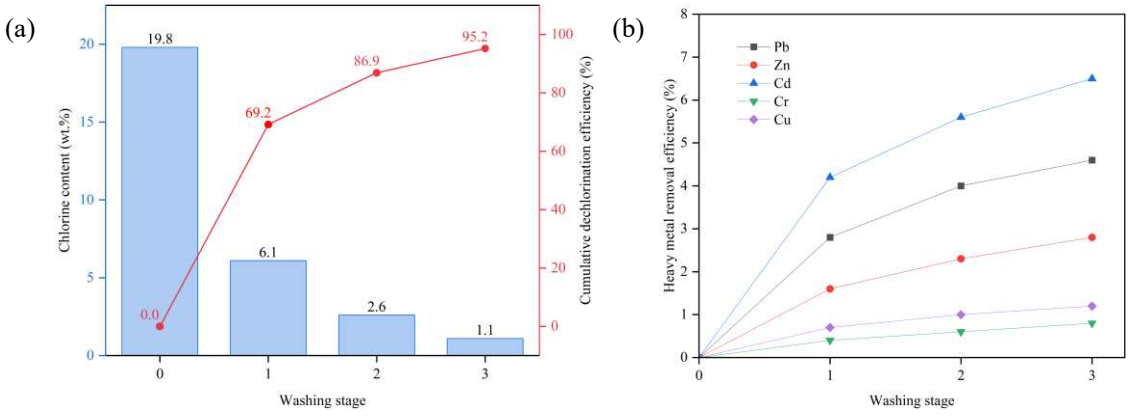

Fig. 2 Effect of three-stage countercurrent water washing on dechlorination and heavy-metal removal from the co-incineration fly ash: (a) Cl content and cumulative dechlorination efficiency; (b) removal efficiencies of Pb, Zn, Cd, Cr, and Cu

3.2 Effect of raw-material ratio on ceramsite properties

At a fixed bottom ash-to-tuff mass ratio of 40:60, increasing the fly ash content from 10% to 40% decreased particle strength from 2210 to 1380 N. The bulk density decreased from 918 to 762 kg/m³, while the 1 h water absorption increased from 5.7% to 21.5% (Fig. 3). A higher fly ash content diluted the SiO_2 and Al_2O_3 framework, while chloride decomposition and the high loss on ignition promoted pore formation. Taking both product performance and fly ash consumption into account, 20% was selected as a suitable dosage.

The property trends with fly ash content reflected two coupled effects. Each increment of fly ash diluted the aluminosilicate framework, because the ash contains only 18.6% SiO_2 + Al_2O_3, and reduced the viscous liquid available for densification. It also increased the chloride and loss-on-ignition loads, so more gas was released during firing. When the liquid phase was insufficient or the gas release was too rapid, open and interconnected pores remained, lowering the bulk density and increasing water absorption [18, 19]. The 10% dosage gave the highest strength and the lowest water absorption, but its fly ash consumption was

limited. At 20%, the strength remained adequate, the bulk density stayed within the 900-grade class, and the residue consumption was doubled relative to 10%. The 20% dosage was therefore selected as a balanced compromise, in line with the optimal fly ash windows reported for other ceramsite systems [9, 11, 17].

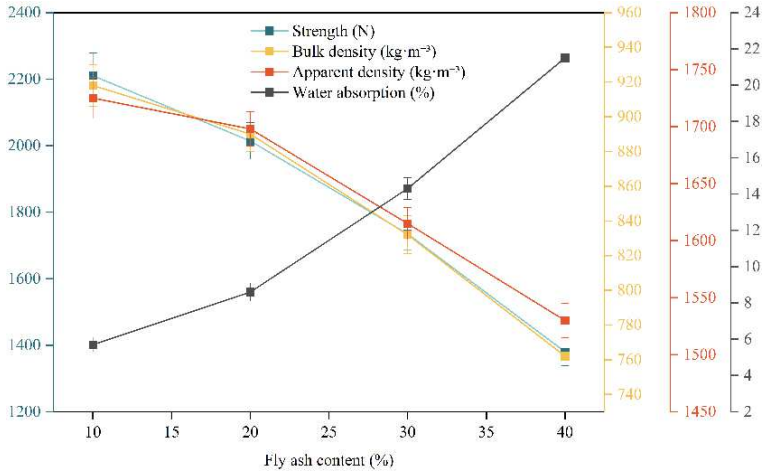

Fig. 3 Effect of fly ash content on ceramsite properties

At 20% fly ash, the optimum bottom ash-to-tuff mass ratio was 40:60, which gave a particle strength of 2014 N, a bulk density of 890 kg/m^3, and a water absorption of 8.6% (Fig. 4). Tuff supplied the silica–alumina framework, whereas the Fe_2O_3, Na_2O, and K_2O in bottom ash promoted liquid formation. Excess bottom ash reduced the framework-forming components and increased the loss on ignition, thereby weakening the product.

The bottom ash-to-tuff mass ratio mainly controlled the SiO_2/Al_2O_3 balance and the amount of fluxing oxides. Tuff contributed 79.94% $SiO_2 + Al_2O_3$ and formed the rigid framework, while bottom ash supplied Fe_2O_3, Na_2O, and K_2O that lowered the melting temperature and promoted liquid formation. At 25:75, the liquid phase was insufficient and the pellets remained under-sintered. At ratios above 40:60, the framework components were diluted and the loss on ignition increased, weakening the product. The 40:60 ratio gave the best combination of strength, density, and water absorption and minimized the bottom ash consumption without exceeding the 900-grade density limit. Similar composition windows have been observed in fly ash-clay and fly ash-slag ternary systems [11, 15].

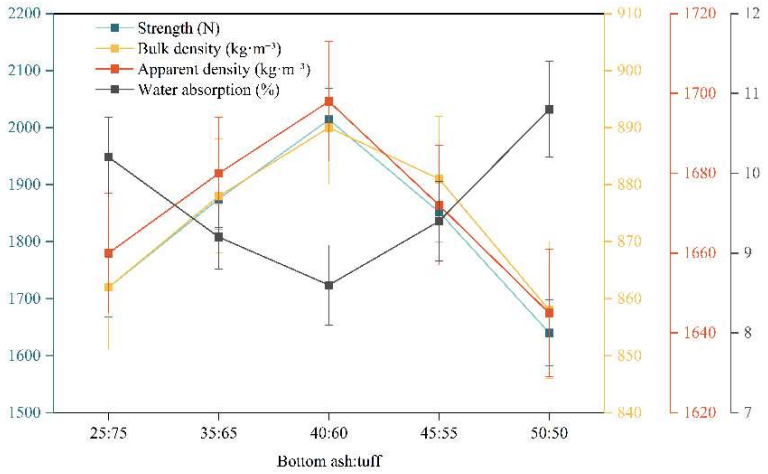

Fig. 4 Effect of bottom ash-to-tuff mass ratio on ceramsite properties

3.3 Effect of firing schedule on ceramsite properties

Raising the preheating temperature from 400 to 600 °C increased particle strength from 1792 to 2146 N and bulk density from 848 to 922 kg/m^3, while water absorption decreased from 12.6% to 4.7% (Fig. 5). Although 600 °C improved strength and water absorption, the bulk density exceeded the upper limit of the 900-grade lightweight aggregate class. A preheating temperature of 500 °C was therefore preferred.

Preheating performed two functions in this process. It gradually burned out residual carbon and volatile organic matter, avoiding the internal pressure build-up that can crack green pellets during rapid heating. It also allowed the solid skeleton to develop before the melt appeared. The strength increase from 1792 N at 400 °C to 2146 N at 600 °C reflected more complete burnout and better preservation of pellet shape at higher preheating temperatures. However, the bulk density at 600 °C reached 922 kg/m³, which exceeds the 900-grade limit of 900 kg/m^3, and the water absorption improved little between 500 and 600 °C. A preheating temperature of 500 °C was therefore chosen to balance burnout with a density margin of about 10 kg/m³ for process fluctuation. Comparable preheating windows have been reported for MSWI fly ash lightweight aggregates [18, 19].

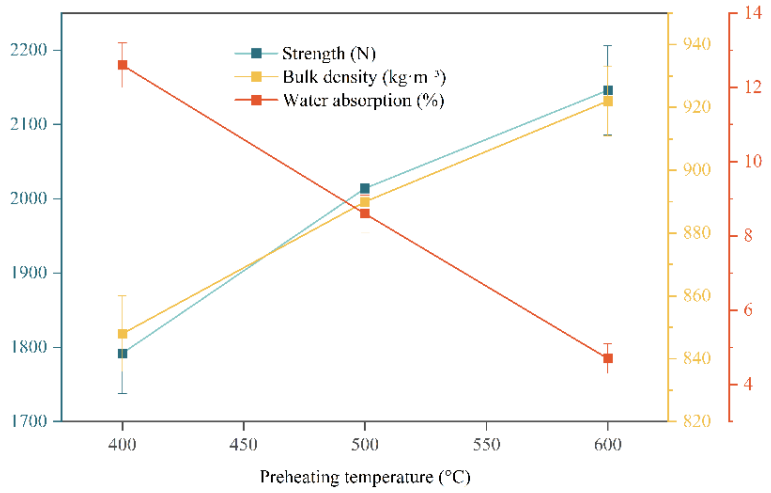

Fig. 5 Effect of preheating temperature on ceramsite properties

The effects of sintering temperature and holding time are shown in Fig. 6. Particle strength reached 2014 N at 1100 °C. At 1050 °C, insufficient liquid formation left open and interconnected pores, producing a low bulk density of 745 kg/m³ and high water absorption. At 1150 °C, excessive liquid caused over-sintering and reduced particle strength to 1668 N. Extending the holding time from 5 to 20 min gradually increased particle strength and bulk density and reduced water absorption, but the improvement slowed after 10 min; 10 min was therefore adopted. The bulk density of the optimal ceramsite was 890 ± 2 kg/m³, leaving a margin of about 10 kg/m³ below the 900-grade upper limit; five validation batches remained within 888–895 kg/m³.

The sintering temperature window was narrow because the liquid-phase behavior changed rapidly with temperature. At 1050 °C, the liquid amount was insufficient and the open pores formed by gas release could not be closed. The bulk density was only 745 kg/m³, and the 1 h water absorption reached 19.8%. At 1150 °C, the liquid became abundant and the pores coalesced into large cavities, which weakened the structure and reduced the particle strength to 1668 N. The strength maximum at 1100 °C therefore corresponds to the condition where the liquid phase closes the open pores without excessive pore coalescence. Holding time played a secondary role: 5 min was too short for complete sintering, while the

improvement between 10 and 20 min was small. The 10 min holding time was adopted to save energy while preserving product stability. The five validation batches remained within 888–895 kg/m³, confirming that the firing window is reproducible [18, 19].

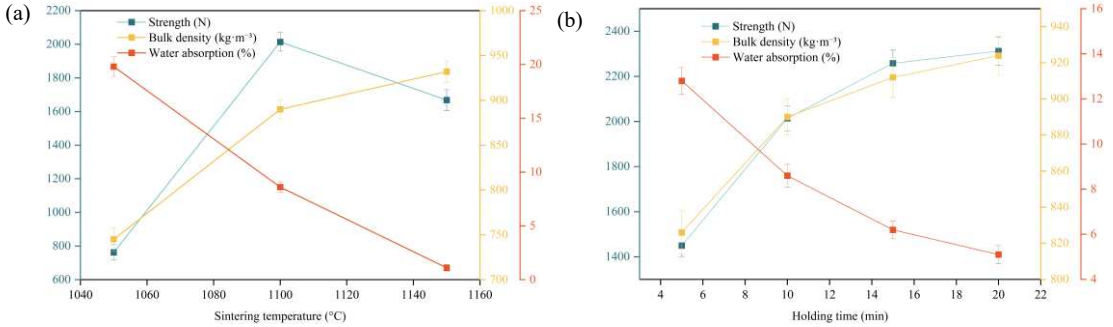

Fig. 6 Effects of sintering temperature and holding time on ceramsite properties: (a) sintering temperature; (b) holding time

3.4 Response-surface optimization and validation

Fly ash content, sintering temperature, and holding time were selected as response-surface variables because the bottom ash-to-tuff ratio and preheating temperature were relatively stable near their optimum levels. A Box–Behnken design was used with particle strength as the response. The coded regression equation is $Y = 2013.0 - 274.8A + 472.4B + 135.1C - 100.7AB - 44.3AC - 55.3BC - 144.5A^2 - 220.1B^2 - 83.3C^2$, where A, B, and C represent fly ash content, sintering temperature, and holding time, respectively.

The model was significant ($R^2 = 0.9922$, adjusted $R^2 = 0.9821$, $F = 98.6$, $p < 0.0001$). The analysis of variance is summarized in Table 6. The predicted R^2 was 0.9410 and the adequate precision was 25.6. Although the lack-of-fit p value (0.065) was close to 0.05, the high R^2 and small pure error supported the use of the model. The influence of the factors followed the order sintering temperature > fly ash content > holding time. The AB interaction was significant, whereas AC and BC were not (Fig. 7). The optimum lay close to the center point, and the predicted gain over the center-point condition was modest; the center-point condition was therefore used in the validation runs. Five validation runs gave a mean strength of 2014 N, close to the predicted value.

The ANOVA results are physically interpretable. Sintering temperature had the largest effect, followed by fly ash content and holding time, in agreement with the single-factor trends. The significant negative AB interaction ($F = 12.3$, $p = 0.0099$) indicates that the benefit of a higher sintering temperature decreased at high fly ash content. A high fly ash content lowers the melt viscosity, so at 1100 °C the pore structure tends to collapse and weaken the aggregate. The significant quadratic terms A^2 and B^2 confirm that both variables have an optimum inside the experimental range. The non-significant AC and BC interactions show that holding time shifted the strength level without changing the response-surface shape. The lack-of-fit p value of 0.065 was only slightly above 0.05, and the small pure error of the center-point replicates supported the model. The validation runs gave a mean strength of 2014 N, close to the predicted value, confirming the reliability of the Box–Behnken model for process control.

Table 6 Analysis of variance for the particle-strength response-surface model

Source	SS	df	MS	F	p	Significance

Model	2917250	9	324139	98.6	<0.0001	***
A-Fly ash content	604180	1	604180	183.8	<0.0001	***
B-Sintering temperature	1785300	1	1785300	542.9	<0.0001	***
C-Holding time	145920	1	145920	44.4	0.0003	***
AB	40560	1	40560	12.3	0.0099	**
AC	7840	1	7840	2.38	0.1666	n.s.
BC	12250	1	12250	3.73	0.0948	n.s.
A^2	88000	1	88000	26.8	0.0013	**
B^2	204000	1	204000	62.1	<0.0001	***
C^2	29200	1	29200	8.88	0.0206	*
Residual	23012	7	3287	—	—	—
Lack of fit	18592	3	6197	5.61	0.065	n.s.
Pure error	4420	4	1105	—	—	—
Total	2940262	16	—	—	—	—

*** $p < 0.001$; ** $p < 0.01$; * $p < 0.05$; n.s. not significant

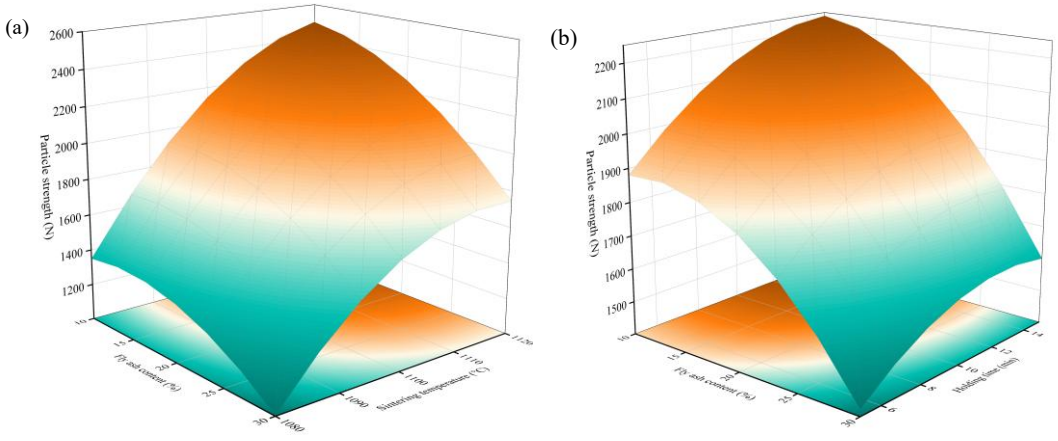

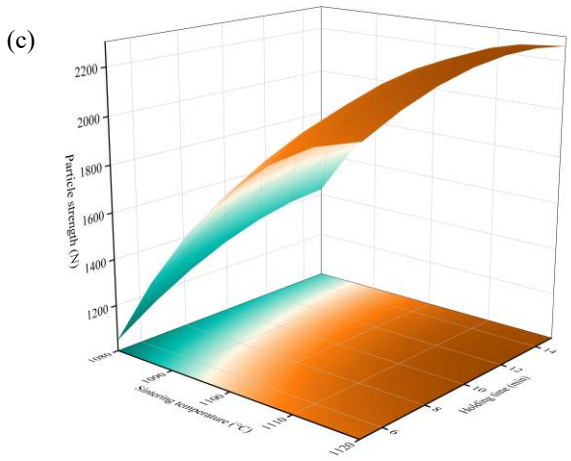

Fig. 7 Response surface and contour plots of particle strength: (a) fly ash content × sintering temperature, holding time fixed at 10 min; (b) fly ash content × holding time, sintering temperature fixed at 1100 °C; (c) sintering temperature × holding time, fly ash content fixed at 20%

3.5 Phase composition and microstructure of the optimal ceramsite

After sintering, the chlorides and carbonates in the fly ash were largely decomposed, and new phases including diopside, hedenbergite, wollastonite, and K-feldspar were formed together with a broad glassy phase. The resulting silicate phases and glassy matrix may encapsulate heavy metals and lower their leachability [9–11, 15]. SEM observations showed a dense surface and predominantly closed, honeycomb-like internal pores with a heterogeneous size distribution, consistent with gas release from chlorides and carbonates and with changes in liquid viscosity during firing [18–20]. The properties of the optimal ceramsite are summarized in Table 7, and its appearance, microstructure, and phase composition are shown in Fig. 8.

The phase evolution can be understood by comparing the raw and sintered mineralogy. The chloride salts and anhydrite in the raw ash decomposed or reacted during firing, while CaO, SiO_2, and Al_2O_3 from the three raw materials combined to form diopside, hedenbergite, wollastonite, and K-feldspar. The formation of these crystalline silicates indicates that the components reacted rather than being physically blended. The broad hump in the XRD pattern corresponds to a glassy phase. Such a phase is typical of alkali- and iron-bearing systems and is considered beneficial for metal encapsulation because it provides a dense matrix with low diffusivity [9, 10, 15]. SEM observation showed a dense external skin and closed, honeycomb-like internal pores. The smooth, partially vitrified pore walls are consistent with gas release while the liquid phase was still sufficiently viscous to retain the pore structure [18, 19]. The dense matrix is expected to incorporate Pb, Cd, and Zn through substitution in silicates or physical encapsulation in glass, although direct evidence from element mapping or synchrotron analysis is still needed [9, 12].

Table 7 Properties of the optimal ceramsite

Property	Mean ± SD	Standard/reference
Particle strength (N)	2014 ± 14	GB/T 17431.2-2010
Bulk density (kg/m³)	890 ± 2	900-grade lightweight aggregate
Apparent density (kg/m³)	1698 ± 3	<2000 kg/m³

1 h water absorption (%)	8.6 ± 0.2	GB/T 17431.2-2010
Crushing strength (MPa)	8.80 ± 0.10	Lytag 4.8–9.1 MPa

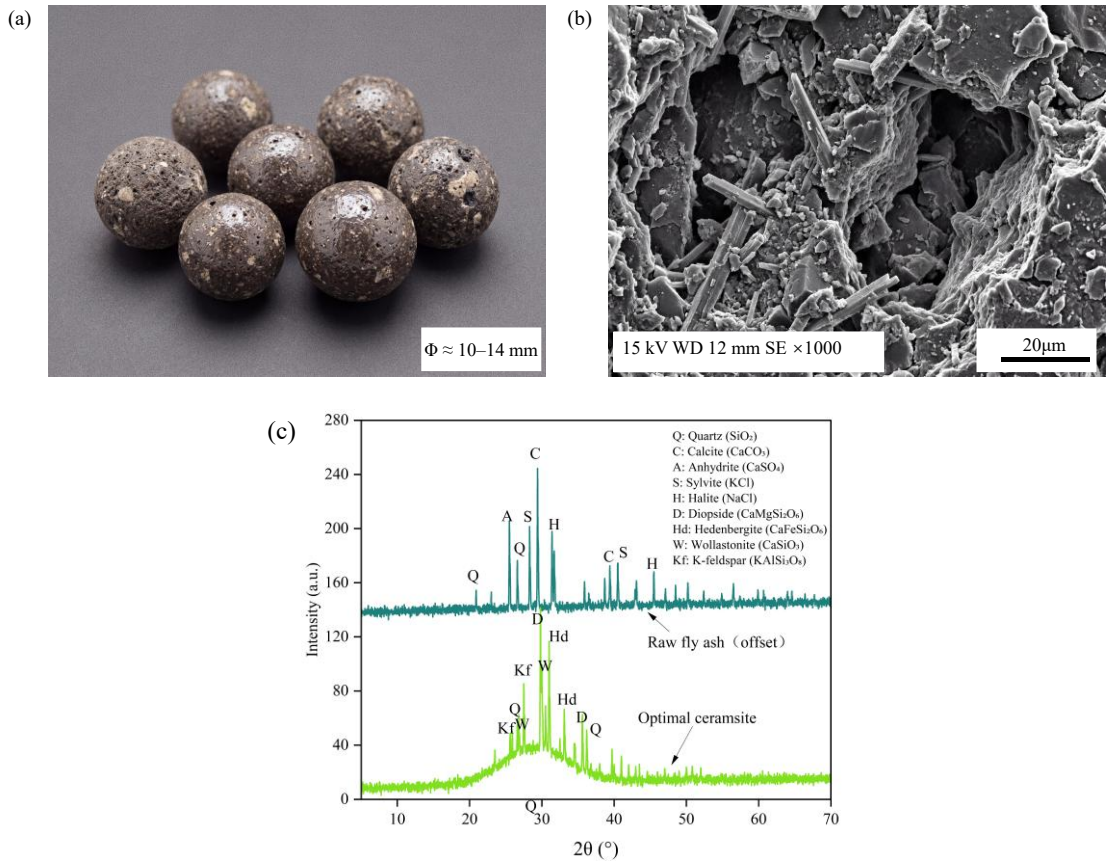

Fig. 8 Appearance, SEM micrographs, and XRD pattern of the optimally prepared ceramsite: (a) macroscopic photograph; (b) SEM micrographs; (c) XRD pattern

3.6 Heavy-metal leaching and environmental safety

Leaching tests were conducted using HJ/T 300-2007 and HJ 557-2010 (Fig. 9). GB 5085.3-2007 and HJ 1134-2020 were used as the primary criteria, and GB 8978-1996 was used only as a reference. In the raw fly ash, the Cd leachate concentration was 4200 μg/L, exceeding the GB 5085.3-2007 limit of 1000 μg/L. The Pb concentration was 3563 μg/L, above the GB 8978-1996 reference limit of 1000 μg/L but below the GB 5085.3 limit of 5000 μg/L. Zn and Cu concentrations were 18500 and 950 μg/L, respectively. After sintering, the optimal ceramsite showed Cd and Pb of 0.5 and 3.2 μg/L under HJ/T 300-2007, and all measured metals were far below the regulatory limits. The decrease in leachability indicates that high-temperature sintering immobilized the metals through phase reconstruction and glass encapsulation, although direct evidence from sequential extraction or EDS mapping is still required.

The two leaching methods provide complementary information. HJ/T 300-2007 uses an acetic acid buffer with a liquid-to-solid ratio of 20:1 and simulates acidic landfill or acid-rain conditions. HJ 557-2010 uses deionized water with a ratio of 10:1 and represents neutral aqueous contact during construction use. In the raw fly ash, the Cd concentration of 4200 μg/L under HJ/T 300-2007 exceeded the GB 5085.3-2007 identification limit of 1000 μg/L, confirming the hazardous nature of the ash. The Pb concentration of 3563 μg/L was below the GB 5085.3 limit of 5000 μg/L but above the GB 8978-1996 reference value of 1000

μg/L. After sintering, the Cd and Pb concentrations decreased to 0.5 and 3.2 μg/L, respectively, and all seven metals were far below the regulatory limits. The reduction is too large to be explained by mass loss or dilution, indicating that the metals were redistributed into less-soluble phases. Leaching tests alone cannot distinguish encapsulation from volatilization to the flue gas; this point is addressed by the preliminary metal balance in Section 3.8. PCDD/Fs were not measured, and their behavior during sintering remains to be confirmed before building-related use.

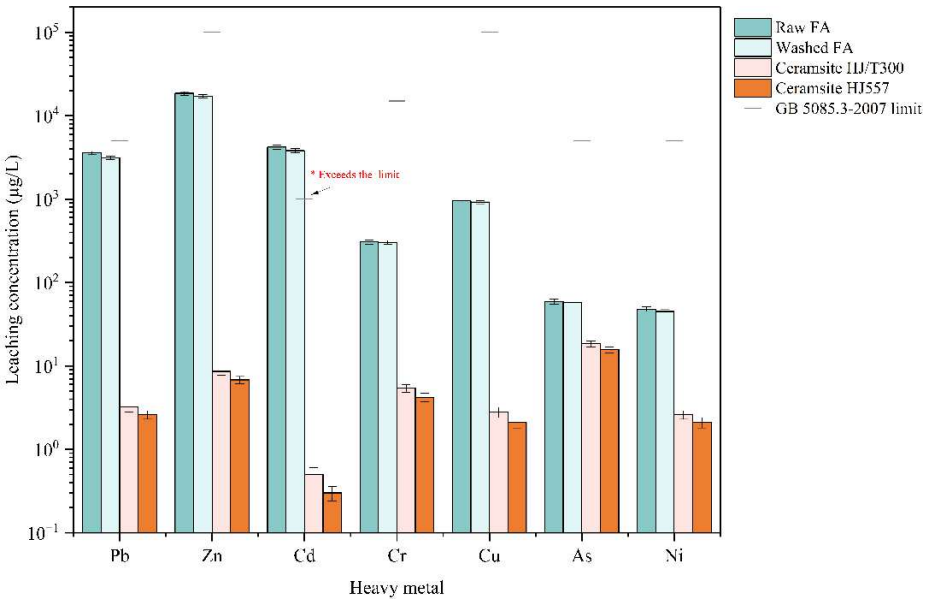

Fig. 9 Heavy-metal leaching concentrations of different samples under HJ/T 300-2007 and HJ 557-2010, with regulatory limits

3.7 Chlorine distribution during water washing and sintering

A chlorine mass balance was established by measuring Cl in the raw fly ash, washed fly ash, ceramsite, washing wastewater, and flue-gas absorption solution (Table 8, Fig. 10). For 200 kg of raw fly ash, washing removed 38.115 kg Cl, corresponding to 96.2% of the total Cl. The actual sintering feed consisted of 135 kg washed fly ash, 400 kg bottom ash, and 400 kg tuff. The total Cl entering sintering was 4.325 kg, comprising 1.485 kg from washed fly ash, 2.04 kg from bottom ash, and 0.80 kg from tuff. Of this, 0.680 kg remained in the ceramsite (15.7%), 3.555 kg entered the flue-gas absorption solution (82.2%), and 0.090 kg was lost analytically (2.1%). No crystalline chlorosilicate or chloroaluminate phase was detected. The chlorine balance is expected to be more complete than the metal balance because HCl is readily absorbed in the alkaline solution, whereas gaseous metal chlorides and submicron aerosols may be only partially captured.

The chlorine balance clarifies the role of the washing step. Washing removed 38.115 kg of the 39.60 kg of chlorine in the raw ash, equivalent to 96.2% on a mass basis, and reduced the chlorine load entering the sintering stage by more than 90%. The sintering feed still contained 4.325 kg of chlorine because bottom ash and tuff contributed 2.04 and 0.80 kg, respectively. Of this amount, 82.2% left the furnace with the flue gas and was captured in the alkaline absorption solution, 15.7% remained in the ceramsite, and 2.1% was analytical loss. The residual chlorine content of the ceramsite was about 0.085%, and no crystalline chlorosilicate or chloroaluminate phase was detected. Residual chlorine therefore exists mainly as soluble salts in the pore solution or as minor species in the glassy phase. Because most chlorine was removed before firing, the risk of heavy-metal chlorination volatilization was reduced, and the flue-gas treatment could be sized for the measured HCl load [4, 15].

391 **Table 8** Chlorine mass balance during washing and sintering

Stage	Stream	Mass (kg)	Cl content (%)	Cl mass (kg)	Fraction of stage Cl (%)	Remark
Washing	Raw fly ash	200	19.8	39.60	100	200 kg raw fly ash
Washing	Washing wastewater	—	—	38.115	96.2	Three-stage countercurrent washing
Washing	Washed fly ash	135	1.1	1.485	3.8	Entering sintering
Sintering input	Washed fly ash	135	1.1	1.485	34.3	Basis of feed
Sintering input	Bottom ash	400	0.51	2.04	47.2	Bottom ash:tuff = 40:60
Sintering input	Tuff	400	0.20	0.80	18.5	Bottom ash:tuff = 40:60
Sintering input	Total input	—	—	4.325	100	1.485 + 2.04 + 0.80
Sintering	Ceramsite residue	800	0.085	0.680	15.7	Cl in ceramsite ≈ 0.085%
Sintering	Flue-gas absorption solution	—	—	3.555	82.2	NaOH absorption of HCl/chlorides
Sintering	Analytical loss	—	—	0.090	2.1	Total ≈ 100%, mass balance closed

Fig. 10 Chlorine distribution during water washing and sintering

3.8 Preliminary distribution of heavy metals between ceramsite and flue gas

To determine whether low leachability reflects safe immobilization, Pb, Cd, and Zn were measured in the raw fly ash, washed fly ash, ceramsite, and flue-gas absorption solution (Fig. 11). The present balance considers only the Pb, Cd, and Zn introduced by the fly ash; the smaller contributions from bottom ash and tuff were not determined. The ceramsite retention ratios were about 85.0%, 70.0%, and 82.0% for Pb, Cd, and Zn, while the flue-gas fractions were about 10.0%, 23.0%, and 15.0%. The washing-wastewater fractions were 4.6%, 6.5%, and 2.8%, and the analytical losses were 0.4%, 0.5%, and 0.2%. The unaccounted fraction may represent gaseous metal chlorides and submicron aerosols not captured by the NaOH/filter sampling.

The preliminary metal balance shows that the retention ratios of Pb, Cd, and Zn in the ceramsite were about 85%, 70%, and 82%, respectively, while the flue-gas fractions were 10%, 23%, and 15%. The order Cd > Zn > Pb in the flue-gas fraction agrees with the volatility of the metal chlorides, because $CdCl_2$ and $ZnCl_2$ have lower boiling points than $PbCl_2$ [4]. The washing fractions were small, 4.6% for Pb, 2.8% for Zn, and 6.5% for Cd. These values are consistent with the speciation results, which show that the metals are mainly associated with carbonates, Fe–Mn oxides, and the residual fraction rather than with soluble chlorides. The unaccounted fraction is attributed to gaseous metal chlorides and submicron aerosols not captured by the NaOH solution and filter. The balance is therefore preliminary and should be verified with standard flue-gas sampling, such as USEPA Method 29/30 or a cascade impactor. Nevertheless, the combination of low leachability and high retention in the ceramsite supports the feasibility of the route, provided that the flue-gas treatment is designed for the measured HCl and metal loads.

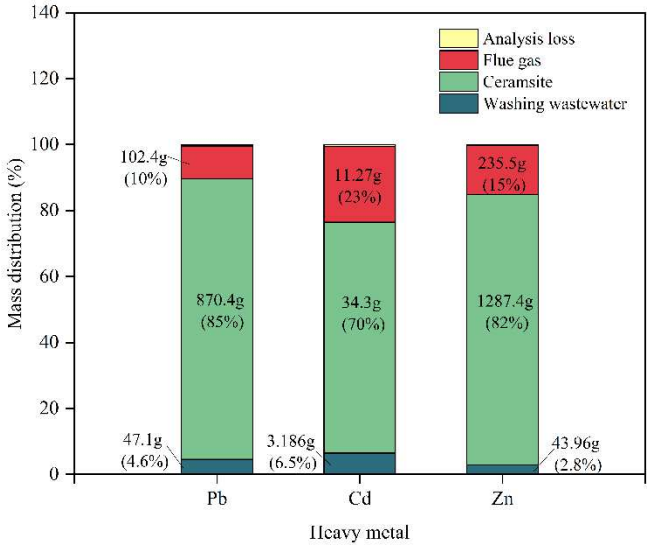

Fig. 11 Preliminary mass distribution of Pb, Cd, and Zn during ceramsite sintering

4 Discussion

The present work extends the ceramsite route from ordinary municipal solid waste incineration fly ash to high-chlorine medical–municipal co-incineration fly ash, with tuff acting as the aluminosilicate framework. Earlier studies have shown that MSWI fly ash can be sintered into lightweight aggregates with clay, ferronickel slag, or dredged sediment [10, 11, 13, 17]. Washing and bloating agents have also been found to improve aggregate quality and metal retention [14, 18–20]. Zhu et al. [15] tracked chlorine migration during the sintering of MSWI fly ash with granite sawing mud, whereas Yang et al. [24] produced geopolymers from bottom ash and tuff without co-incineration fly ash. The present system differs in two respects. It combines co-incineration fly ash, bottom ash, and tuff in one ternary system, and it closes both the chlorine and the heavy-metal balances from the raw ash through the product and flue gas. The resulting 900-grade ceramsite, with a particle strength of 2014 N and a bulk density of 890 kg/m³, is comparable to aggregates reported for MSWI fly ash-based systems (Table 9) [9, 11, 17].

Table 9 Comparison of ceramsite properties reported in this study and representative fly-ash ceramsite studies

Study	Feedstock	Sintering temperature (°C)	Bulk density (kg/m³)	1 h water absorption (%)	Strength (MPa)
This study	Medical–municipal co-incineration fly ash, bottom ash, tuff	1100	890	8.6	8.80 (crushing)
Shao et al. [9]	MSWI fly ash, civil sludge, contaminated soil, clay	1150	998.7	0.97	37.84 (compressive)

Han et al. [18]	MSWI fly ash, clay, SiC	1120	212	NR	NR
Han et al. [19]	Washed MSWI fly ash, bentonite, SiC	1140–1160	NR	NR	NR

NR: not reported in the cited source.

Chlorine was the main constraint in this system. The raw fly ash contained 19.8% Cl, and three-stage countercurrent washing removed 96.2% of the chlorine on a mass basis. This pretreatment lowered the chlorine load entering the sintering stage by more than 90%, reduced the risk of chlorination volatilization of Pb, Cd, and Zn, and left only about 0.085% Cl in the product. The mass balance showed that 82.2% of the chlorine in the sintering feed was released to the flue gas and captured in the alkaline absorption solution. Flue-gas deacidification is therefore an integral part of the process rather than an optional add-on. Compared with direct sintering of unwashed ash, the washing-sintering combination allows the HCl load and the metal emissions to be managed separately, which simplifies the design of the flue-gas treatment train [15, 25, 26].

The heavy-metal results support the environmental feasibility of the route, with two caveats. The leachate concentrations of Pb, Cd, Zn, Cr, Cu, As, and Ni in the optimal ceramsite were far below the GB 5085.3-2007 and HJ 1134-2020 limits. The preliminary mass balance indicated that 70–85% of the Pb, Cd, and Zn introduced by the fly ash remained in the ceramsite. However, the flue-gas fractions were probably underestimated because gaseous metal chlorides and submicron aerosols are only partially captured by the NaOH solution and filter sampling. The retention ratios should therefore be verified with standard methods such as USEPA Method 29/30 or a cascade impactor before the material is promoted as safe. The reduction in leachability is likely related to phase reconstruction and glass encapsulation, a common interpretation in fly ash ceramsite studies [9, 10, 12]. Direct speciation evidence for the sintered product, such as sequential extraction, EDS mapping, or XAFS, is still required.

Two limitations should be acknowledged. PCDD/Fs were not measured in this work. Thermal treatment generally favors their decomposition [3, 5], but their degradation and possible re-formation during sintering must be confirmed before building-related applications are proposed. The density margin of the 900-grade product is also narrow. The bulk density of 890 kg/m³ leaves only about 10 kg/m³ below the upper limit. Raw-material fluctuations, such as seasonal changes in the medical waste ratio or chloride content, could therefore push the product out of grade. Pilot-scale trials are needed to evaluate process robustness, and the flue-gas metal sampling should be improved in these trials.

Several directions follow from this study. Mechanistically, identifying the binding sites of Pb, Cd, and Zn in the silicate and glassy phases would strengthen the immobilization claim. From an engineering perspective, the water-washing wastewater, flue-gas deacidification, and product certification should be evaluated together at pilot scale. A life-cycle assessment would show whether the energy input for washing and sintering is offset by the avoided landfilling of hazardous ash and the substitution of natural aggregates. The measured chlorine and metal distributions also provide quantitative input for the design of full-scale plants. The proposed route thus offers a technically feasible basis for the high-value utilization of medical–municipal co-incineration ash, while the remaining environmental and economic questions define the agenda for scale-up studies.

5 Conclusion

This study developed a lightweight ceramsite route for medical–municipal co-incineration fly ash by combining three-stage countercurrent water-washing dechlorination with ternary sintering using bottom ash

and tuff. The optimal formulation was 20% fly ash with a bottom ash-to-tuff mass ratio of 40:60. The optimal firing schedule was preheating at 500 °C for 20 min and sintering at 1100 °C for 10 min. The product was a 900-grade lightweight aggregate with a particle strength of 2014 N, a bulk density of 890 kg/m³, and a 1 h water absorption of 8.6%. The route also reduced the demand for clay as a raw material by using locally available tuff.

During sintering, chloride and carbonate phases decomposed, and diopside, hedenbergite, wollastonite, and K-feldspar formed together with a glassy phase. The chlorine mass balance was nearly closed. Washing removed 96.2% of the chlorine in the raw fly ash. Of the chlorine entering the sintering stage, 82.2% was released to the flue gas and captured in the alkaline absorption solution. The remaining chlorine was retained in the ceramsite (15.7%) or lost analytically (2.1%). The leachate concentrations of Pb, Cd, Zn, Cr, Cu, As, and Ni in the ceramsite were far below the GB 5085.3-2007 and HJ 1134-2020 limits. A preliminary balance indicated that 70–85% of the Pb, Cd, and Zn introduced by the fly ash remained in the product.

These retention ratios should be regarded as apparent values because gaseous metals may be underestimated by the present sampling method. The flue-gas fractions should therefore be verified with standard sampling techniques. The reduction in heavy-metal leachability is likely associated with phase reconstruction and glass encapsulation, but direct speciation evidence for the sintered product is still required. The proposed route offers a technically feasible basis for the high-value utilization of medical–municipal co-incineration ash. Before industrial application, standard flue-gas metal sampling, sequential extraction and EDS/XAFS analysis, PCDD/Fs measurement, and pilot-scale life-cycle assessment should be conducted.

Acknowledgements

We thank the staff who provided assistance in sampling and investigations in the selected sites.

Statements and Declarations

Funding: This work was supported by the Key Scientific Research Project Plan of Henan Provincial Higher Education Institutions (2026) (Grant No. 26B610009) and a project entitled “Key Technologies for High-Value Utilization of Medical-Municipal Waste Incineration Ash and Slag Synergistically with Tuff”.

Competing interests: The authors declare that they have no competing interests.

Data availability: The datasets generated and/or analyzed during the current study are available from the corresponding author upon reasonable request.

Ethics approval and consent to participate: Not applicable.

Consent for publication: All authors have read and agreed to the published version of the manuscript.

CRediT authorship contribution statement: Junyang Teng: Writing – original draft, Software, Formal analysis, Data curation, Funding acquisition. Yonghao Yang: Writing – original draft, Software, Formal analysis, Data curation. Fei Xu: Writing – original draft, Software, Formal analysis, Data curation.

References

1. Liu F, Liu H, Wei G, Zhang R, Zeng T, Liu G, Zhou J (2018) Characteristics and treatment methods of medical waste incinerator fly ash: a review. Processes 6:173. doi: 10.3390/pr6100173

2. Bolan S, Padhye LP, Kumar M, Antoniadis V, Sridharan S, Tang Y, Singh N, Hewawasam C, Vithanage M, Singh L, et al. (2023) Review on distribution, fate, and management of potentially toxic elements in incinerated medical wastes. Environ Pollut 321:121080. doi: 10.1016/j.envpol.2023.121080

3. Zhang C, Bai Z, Liu X, Xia D, Li X, Long J, Sun Z, Li Y, Sun Y (2024) Co-incineration of medical waste in municipal solid waste incineration increased emission of chlorine/brominated organic pollutants. Sci Total Environ 937:173544. doi: 10.1016/j.scitotenv.2024.173544

4. Shen W, Zhu N, Xi Y, Huang J, Li F, Wu P, Dang Z (2022) Effects of medical waste incineration fly ash on the promotion of heavy metal chlorination volatilization from incineration residues. J Hazard Mater 425:128037. doi: 10.1016/j.jhazmat.2021.128037

5. Song H, Huang Y, Pang J, Li Z, Zhu Z, Cheng H, Gao J, Zuo W, Zhou H (2024) A study of the stabilization and solidification of heavy metals in co-vitrification of medical waste incineration ash and coal fly ash. Waste Manag 186:46-54. doi: 10.1016/j.wasman.2024.06.003

6. Liu R, Liu S, Sun S, Cao X, Lin J, Peng J, Ji F, Ma R (2024) Medical waste incineration fly ash-based magnesium potassium phosphate cement: calcium-reinforced chlorine solidification/stabilization mechanism and optimized carbon reduction process strategy. J Environ Manage 357:120749. doi: 10.1016/j.jenvman.2024.120749

7. Tzanakos K, Mimilidou A, Anastasiadou K, Stratakis A, Gidarakos E (2014) Solidification/stabilization of ash from medical waste incineration into geopolymers. Waste Manag 34:1823-1828. doi: 10.1016/j.wasman.2014.03.021

8. Fan C, Wang B, Ai H, Qi Y, Liu Z (2021) A comparative study on solidification/stabilization characteristics of coal fly ash-based geopolymer and Portland cement on heavy metals in MSWI fly ash. J Clean Prod 319:128790. doi: 10.1016/j.jclepro.2021.128790

9. Shao Y, Shao Y, Zhang W, Zhu Y, Dou T, Chu L, Liu Z (2022) Preparation of municipal solid waste incineration fly ash-based ceramsite and its mechanisms of heavy metal immobilization. Waste Manag 143:54-60. doi: 10.1016/j.wasman.2022.02.021

10. Wu X, Gu F, Su C, Wang W, Pu K, Shen D, Long Y (2022) Preparing high-strength ceramsite from ferronickel slag and municipal solid waste incineration fly ash. Ceram Int 48:34265-34272. doi: 10.1016/j.ceramint.2022.07.357

11. Long Y, Pu K, Yang Y, Huang H, Fang H, Shen D, Geng H, Ruan J, Gu F (2023) Preparation of high-strength ceramsite from municipal solid waste incineration fly ash and clay based on CaO-SiO_2-Al_2O_3 system. Constr Build Mater 368:130492. doi: 10.1016/j.conbuildmat.2023.130492

12. Shi Y, Li Y, Yuan X, Fu J, Ma Q, Wang Q (2020) Environmental and human health risk evaluation of heavy metals in ceramsites from municipal solid waste incineration fly ash. Environ Geochem Health 42:3779-3794. doi: 10.1007/s10653-020-00639-7

13. Deng X, Jian R, Chen S, Wang X, Wan C, Xue Y, Wang T (2023) Killing two birds with one stone: preparation of ceramsite high-strength lightweight aggregate via co-sintering of dredged sediment and municipal solid waste incinerated fly ash. Constr Build Mater 409:134039. doi: 10.1016/j.conbuildmat.2023.134039

14. Huang J, Chu X, Shu Z, Ma X, Jin Y (2023) The effects of washing solvents on the properties of ceramsite and heavy metal immobilization via the cosintering of municipal solid waste incineration fly ash and Cr-containing waste glass. J Environ Chem Eng 11:109089. doi: 10.1016/j.jece.2022.109089

15. Zhu Y, Shao Y, Tian C, Zhang W, Zhang T, Shao Y, Ma J (2024) Preparation of municipal solid waste incineration fly ash/granite sawing mud ceramsite and the morphological transformation and migration properties of chlorine. Waste Manag 173:1-9. doi: 10.1016/j.wasman.2023.10.039

16. Han A, Wang R, Zhang C, Wang H, Wang Z (2025) Preparation of ceramsite from heavy metal contained municipal solid waste incineration fly ash synergistically with silicon/aluminum-containing waste. J Hazard Mater Adv 18:100725. doi: 10.1016/j.hazadv.2025.100725

17. Ferraro A, Ducman V, Colangelo F, Korat L, Spasiano D, Farina I (2023) Production and characterization of lightweight aggregates from municipal solid waste incineration fly-ash through single- and double-step pelletization process. J Clean Prod 383:135275. doi: 10.1016/j.jclepro.2022.135275

18. Han S, Song Y, Ju T, Meng Y, Meng F, Song M, Lin L, Liu M, Li J, Jiang J (2022) Recycling municipal solid waste incineration fly ash in super-lightweight aggregates by sintering with clay and using SiC as bloating agent. Chemosphere 307:135895. doi: 10.1016/j.chemosphere.2022.135895

19. Han S, Ju T, Meng F, Lin L, Li J, Chen K, Jiang J (2023) Comprehensive study of recycling municipal solid waste incineration fly ash in lightweight aggregate with bloating agent: effects of water washing and bloating mechanism. Sci Total Environ 881:163267. doi: 10.1016/j.scitotenv.2023.163267

20. Han S, Chen K, Meng F, Gao Y, Li J, Lin L, Qin W, Jiang J (2023) pH-controlled sulfuric acid washing enhancing heavy metal stabilization in lightweight aggregate production from municipal solid waste incineration fly ash. J Clean Prod 430:139774. doi: 10.1016/j.jclepro.2023.139774

21. Tan W, Lv J, Deng Q, Zhang X (2016) Application of a combination of municipal solid waste incineration fly ash and lightweight aggregate in concrete. J Adhes Sci Technol 30:866-877. doi: 10.1080/01694243.2015.1128179

22. Wei N (2015) Leachability of heavy metals from lightweight aggregates made with sewage sludge and municipal solid waste incineration fly ash. Int J Environ Res Public Health 12:4992-5005. doi: 10.3390/ijerph120504992

23. Tekin I (2016) Properties of NaOH activated geopolymer with marble, travertine and volcanic tuff wastes. Constr Build Mater 127:607-617. doi: 10.1016/j.conbuildmat.2016.10.038

24. Yang Y, Luo Z, Huang F, Ni C, Wu J, Zheng B (2024) Utilizing municipal solid waste incineration bottom ash and volcanic tuff to produce geopolymer materials. Constr Build Mater 425:136015. doi: 10.1016/j.conbuildmat.2024.136015

25. Chen X, Bi Y, Zhang H, Wang J (2016) Chlorides removal and control through water-washing process on MSWI fly ash. Procedia Environ Sci 31:560-566. doi: 10.1016/j.proenv.2016.02.086

26. Zuo W, Zhao R, Dong G, Ma G, Zhou H, Song T, Tu Y, Xie H, Wang X (2022) CO_2-assisted water-washing process of municipal solid waste incineration fly ash for chloride removal. Energy Fuels 36:13732-13742. doi: 10.1021/acs.energyfuels.2c03014

27. GB/T 17431.2-2010 (2010) Lightweight aggregates and its test methods. Part 2: Test methods for lightweight aggregates. Standards Press of China, Beijing

28. HJ/T 300-2007 (2007) Solid waste. Extraction procedure for leaching toxicity. Acetic acid buffer solution method. China Environmental Science Press, Beijing

29. HJ 557-2010 (2010) Solid waste. Extraction procedure for leaching toxicity. Horizontal vibration method. China Environmental Science Press, Beijing

30. HJ 1134-2020 (2020) Technical specification for pollution control of fly ash from municipal solid waste incineration. China Environmental Science Press, Beijing

31. GB 5085.3-2007 (2007) Identification standards for hazardous wastes. Identification for extraction toxicity. Standards Press of China, Beijing

32. GB 8978-1996 (1996) Integrated wastewater discharge standard. Standards Press of China, Beijing

Supplementary Files

This is a list of supplementary files associated with this preprint. Click to download.

- Highlights.docx